

Direct Estimation of Appearance Models for Segmentation*

Jeova F. S. Rocha Neto[†]

Pedro Felzenszwalb[‡]

Marilyn Vazquez[‡]

December 23, 2024

Abstract

Image segmentation algorithms often depend on appearance models that characterize the distribution of pixel values in different image regions. We describe a novel approach for estimating appearance models directly from an image, without explicit consideration of the pixels that make up each region. Our approach is based on algebraic expressions that relate local image statistics to the appearance models of spatially coherent regions. We describe two algorithms that can use the aforementioned algebraic expressions for estimating appearance models. The first algorithm is based on solving a system of linear and quadratic equations. The second algorithm is a spectral method based on an eigenvector computation. We present experimental results that demonstrate the proposed methods work well in practice and lead to effective image segmentation algorithms.

Keywords: Image segmentation, Mixture models, Markov Random Fields

MSC: 68U10, 62M05, 62H30, 65C20

1 Introduction

Image segmentation is a fundamental problem in computer vision and image processing. The goal of segmentation is to partition an image into regions corresponding to different objects or materials that are visible in a scene. There are numerous applications of automatic segmentation methods including in medical image analysis, remote sensing, industrial inspection, object recognition and interactive image editing. Therefore, advances in image segmentation can have significant impact in many applications.

Segmentation algorithms often rely on some type of appearance modeling to be able to classify each pixel in the image into different regions. Many segmentation algorithms are based on minimization of functionals that encourage spatial coherence of regions and a fit of the pixels in each region to an appearance model.

In some settings such as medical image analysis or remote sensing the appearance of different objects of interest may be known in advance. On the other hand, in many applications the appearance of the objects or materials in a scene need to be determined during the segmentation process.

When appearance models are not known in advance, the challenge of image segmentation is that it is essentially a “chicken-and-egg” problem. If we had appearance models we could segment the image. On the other hand, if we had a segmentation we could estimate the appearance of each region. Some methods such as [1] and [2] alternate between estimating appearance models and estimating a segmentation in an iterative fashion. Similarly, variational methods such as [3] and [4] repeatedly evolve a segmentation and the appearance model of each region. Less frequently, methods such as [5] and [6] tackle the segmentation problem by making the dependency on appearance models implicit.

In this paper we describe a novel approach for estimating appearance models directly from an image, without explicit consideration of the pixels in each image region. The approach relies on the spatial coherence of regions but does not require solving for a segmentation to determine the appearance of each region. Instead

*This material is based upon work supported by the National Science Foundation under Grant No. DMS-1439786 while the authors were in residence at the Institute for Computational and Experimental Research in Mathematics in Providence, RI, during the Spring 2019 semester.

[†]School of Engineering, Brown University, Providence, RI, USA

[‡]Mathematical Bioscience Institute, Ohio State University, Columbus, OH, USA

we derive a set of algebraic expressions that can be used to solve for the appearance models of each region using local statistics that can be easily estimated directly from an image.

Our results allow for the development of new segmentation algorithms that use a two-step process for segmentation. First we determine appearance models without segmenting the image. We can then segment the image using any available method that requires appearance models to be fixed in advance. In practice we propose to use the estimated appearance models to define a Markov Random Field [7], and use efficient graph cut algorithms to segment the image [8, 9]. This two-step approach leads to efficient methods for unsupervised segmentation.

Many image segmentation algorithms pre-process an image using the response of Gabor filters to define features [10, 11, 12]. Although very useful for capturing texture information, the use of filter banks requires significant processing and memory overhead. Moreover, the use of filter responses as features for segmentation leads to inaccurate localization of region boundaries, due to the non-trivial spatial extent of texture filters.

The algorithms we describe in this paper allow for estimating non-parametric appearance models that can represent the appearance of textures directly in terms of individual pixel values. This makes it possible to segment images with textures without relying on filter banks. This leads to efficient methods that accurately localize the boundaries between regions with complex textures.

The remainder of the paper is organized as follows. In Section 2 we describe how we represent the appearance of regions using non-parametric statistical models. In Section 3 we discuss how local image statistics can be related to appearance models using algebraic equations. These algebraic equations lead to two different methods for estimating appearance models described in Section 4. In Section 5, we show experimental results and evaluate both the accuracy of the estimated appearance models and the segmentations obtained using these models. Finally, Section 6 concludes the paper with a summary and brief discussion.

2 Appearance Models for Segmentation

Let $I : \Omega \rightarrow L$ be an image, where Ω is a set of pixel locations and L is a finite set of pixel values. For an n by m graylevel image we have $\Omega = \{1, \dots, n\} \times \{1, \dots, m\}$ while $L = \{0, \dots, 255\}$. In Section 5.6, we will discuss how to generalize our methods to RGB images. We use $I(x)$ to denote the value of a pixel $x \in \Omega$. A region \mathcal{R} is a subset of the pixels in Ω .

We define an *appearance model* $\theta \in \mathbb{R}^L$ to be a distribution over L . An appearance model for a region \mathcal{R} specifies the typical values for the pixels in \mathcal{R} . Note, however, that an appearance model θ does not fully specify the joint distribution of the pixels in a region, only the frequencies of different pixel values. We do not assume the pixel values in each region are independent. Therefore the appearance models considered here only define a coarse representation for the appearance of a region. For example, if we permute the pixels within a region the appearance model would remain the same.

We assume the image I can be divided into two regions \mathcal{R}_0 and \mathcal{R}_1 and use $S : \Omega \rightarrow \{0, 1\}$ to denote a binary image specifying an assignment of image pixels into regions, or a *segmentation*. Let w_0 and w_1 be the areas of the two regions, normalized to sum to one. That is, $w_0 = |\mathcal{R}_0|/|\Omega|$ and $w_1 = |\mathcal{R}_1|/|\Omega|$. Finally, let θ_0 and θ_1 be appearance models for the pixels in each region.

As discussed in the introduction, one of the fundamental challenges of unsupervised image segmentation is that it is essentially a “chicken-and-egg” problem. If we have appearance models θ_0 and θ_1 we can partition the image into regions using several existing approaches. On the other hand, if we have a partition of an image into regions \mathcal{R}_0 and \mathcal{R}_1 we can estimate appearance models by computing histograms of the pixel values in each region.

The main contribution of our work is a method for estimating the appearance models θ_0 and θ_1 *directly* from an image, without explicit consideration of the regions \mathcal{R}_0 and \mathcal{R}_1 .

Once appearance models are estimated there are many methods that can be used to partition an image. In the simplest setting we can classify each pixel independently using a likelihood ratio defined by θ_0 and θ_1 . Alternatively, methods based on Markov Random Fields ([7]) segment an image by minimizing an energy that combines the appearance models with a boundary regularization term,

$$E(S|\lambda, \theta_0, \theta_1) = - \sum_{x \in \Omega} \ln \theta_{S(x)}(I(x)) + \lambda \sum_{x, y \text{ neighbors}} |S(x) - S(y)|. \quad (1)$$

In this case the minimum energy segmentation corresponds to a MAP estimate of S , where the boundary regularization defines a prior over segmentations. Importantly, the energy function E can be efficiently minimized by the computation of a minimum cut in a graph ([8]).

3 Image Statistics

In order to approach the appearance model estimation problem, we treat the image as a random field and consider two distributions that can be directly estimated from an observed image. The first distribution, α , captures the frequencies of pixel values in the image. The second distribution, β , captures the frequencies of pairs of pixel values at a fixed distance, r , from each other.

Let $\alpha \in \mathbb{R}^L$ be a distribution over L where $\alpha(i)$ is the probability that a pixel $x \in \Omega$ selected uniformly at random has value i ,

$$\alpha(i) = P(I(x) = i).$$

Let $\beta \in \mathbb{R}^{L \times L}$ be a distribution over $L \times L$ where $\beta(i, j)$ is the probability that two pixels $x, y \in \Omega$ with $\|x - y\| = r$ selected uniformly at random have values i and j respectively,

$$\beta(i, j) = P(I(x) = i, I(y) = j).$$

Since the pixels are in a discrete grid we use the L1 norm to measure the distance between them and round r to an integer to avoid digitization artifacts.

Note that we can easily estimate α and β from an observed image. To estimate α we count the fraction of pixels that have a particular value. To estimate β we count the fraction of pairs of pixels at distance r from each other that have a particular pair of values. If the image is large we can also estimate the two distributions using a random sample of pixels and a random sample of pairs of pixels at distance r . We use $\hat{\alpha}$ and $\hat{\beta}$ to denote the estimates of α and β computed from an observed image.

Let \mathcal{R}_0 and \mathcal{R}_1 be a partition of Ω into two regions. Let $x, y \in \Omega$ be two pixels with $\|x - y\| = r$ selected uniformly at random and consider the probability that x and y are in different regions. Since x and y are exchangeable, let $\epsilon_r = P(x \in \mathcal{R}_0, y \in \mathcal{R}_1) = P(x \in \mathcal{R}_1, y \in \mathcal{R}_0)$. This means that the probability of x and y being in different regions is $2\epsilon_r$.

Let w_0 and w_1 be the areas of the regions \mathcal{R}_0 and \mathcal{R}_1 normalized to sum to one. Finally, let θ_0 and θ_1 be distributions over L defining appearance models for the two regions.

We will relate α and β to $w_0, w_1, \theta_0, \theta_1$ and ϵ_r using two key assumptions. The first assumption is that regions have homogeneous appearance in the following sense.

Assumption 1 (Homogeneity). *The probability that a pixel takes a particular value depends only on the region the pixel belongs to,*

$$P(I(x) = i | x \in \mathcal{R}_s) = \theta_s(i).$$

Note that this assumption does not specify a full generative model for the image. We assume the pixels in each region have the same marginal distribution, but their joint distribution could involve dependencies, as we see for example in images with textures. Similar assumptions have been used in other approaches for image segmentation, including several methods for unsupervised texture segmentation [4, 12, 11].

The second assumption captures the idea that sufficiently far away pixels are independent.

Assumption 2 (Independence at a distance). *If x and y are two pixels with $\|x - y\| = r$ then,*

$$P(I(x) = i, I(y) = j | x \in \mathcal{R}_s, y \in \mathcal{R}_t) = P(I(x) = i | x \in \mathcal{R}_s)P(I(y) = j | y \in \mathcal{R}_t).$$

For images with a single region Assumption 2 is equivalent to $\beta = \alpha\alpha^\top$. Figure 1 evaluates this assumption in textured images from the Brodatz dataset [13]. See Figure 5 for examples of the images in the Brodatz dataset. In this case each image has a single region and we compare $\hat{\beta}$ to $\hat{\alpha}\hat{\alpha}^\top$ for different values of r . When r is small we see that the two distributions, $\hat{\beta}$ and $\hat{\alpha}\hat{\alpha}^\top$, are quite different, because nearby pixels are not independent. As we increase r we see that $\hat{\beta}$ is close to $\hat{\alpha}\hat{\alpha}^\top$, suggesting that pixels that are relatively far from each other are independent.

The following proposition shows how the two assumptions above lead to algebraic expressions relating α and β to $w_0, w_1, \theta_0, \theta_1$ and ϵ_r . These algebraic expressions will enable us to estimate θ_0 and θ_1 without explicit consideration of \mathcal{R}_0 and \mathcal{R}_1 .

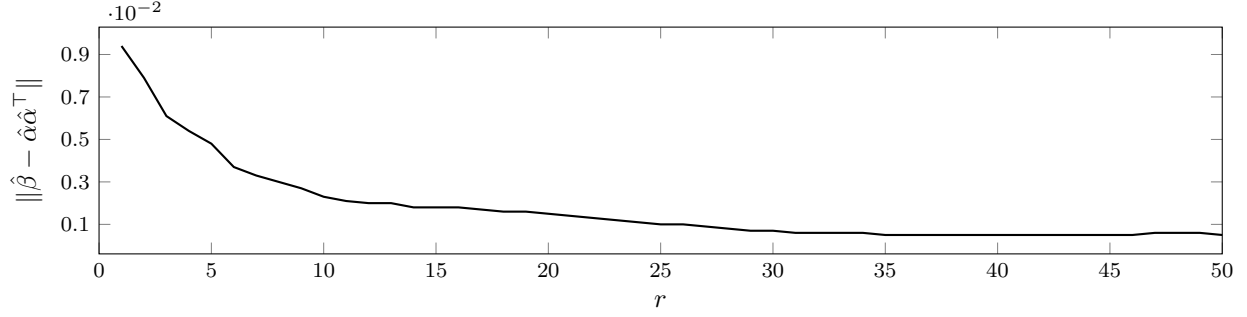


Figure 1: Evaluating independence at a distance. We show the difference between $\hat{\beta}$ and $\hat{\alpha}\hat{\alpha}^\top$ as r increases for images with a single texture. The graph depicts the averages over all Brodatz textures.

Proposition 1. *Under Assumptions 1 and 2 we have:*

$$\alpha = w_0\theta_0 + w_1\theta_1. \quad (2)$$

$$\beta = (w_0 - \epsilon_r)\theta_0\theta_0^\top + (w_1 - \epsilon_r)\theta_1\theta_1^\top + \epsilon_r\theta_0\theta_1^\top + \epsilon_r\theta_1\theta_0^\top. \quad (3)$$

Proof. For (2) let x be a pixel selected uniformly at random. Then,

$$\begin{aligned} \alpha(i) &= P(I(x) = i) \\ &= P(x \in \mathcal{R}_0)P(I(x) = i | x \in \mathcal{R}_0) + P(x \in \mathcal{R}_1)P(I(x) = i | x \in \mathcal{R}_1) \\ &= w_0\theta_0(i) + w_1\theta_1(i) \end{aligned}$$

For (3) let x and y be two pixels with $\|x - y\| = r$ selected uniformly at random. Note that

$$P(x \in \mathcal{R}_0) = P(x \in \mathcal{R}_0, y \in \mathcal{R}_0) + P(x \in \mathcal{R}_0, y \in \mathcal{R}_1).$$

Therefore $P(x \in \mathcal{R}_0, y \in \mathcal{R}_0) = w_0 - \epsilon_r$. Similarly $P(x \in \mathcal{R}_1, y \in \mathcal{R}_1) = w_1 - \epsilon_r$. Now,

$$\begin{aligned} \beta(i, j) &= P(I(x) = i, I(y) = j) \\ &= P(x, y \in \mathcal{R}_0)P(I(x) = i, I(y) = j | x, y \in \mathcal{R}_0) + \\ &\quad P(x, y \in \mathcal{R}_1)P(I(x) = i, I(y) = j | x, y \in \mathcal{R}_1) + \\ &\quad P(x \in \mathcal{R}_0, y \in \mathcal{R}_1)P(I(x) = i, I(y) = j | x \in \mathcal{R}_0, y \in \mathcal{R}_1) + \\ &\quad P(x \in \mathcal{R}_1, y \in \mathcal{R}_0)P(I(x) = i, I(y) = j | x \in \mathcal{R}_1, y \in \mathcal{R}_0) \\ &= (w_0 - \epsilon_r)\theta_0(i)\theta_0(j) + (w_1 - \epsilon_r)\theta_1(i)\theta_1(j) + \epsilon_r\theta_0(i)\theta_1(j) + \epsilon_r\theta_1(i)\theta_0(j) \end{aligned}$$

□

4 Appearance Estimation

4.1 Algebraic Method

As discussed in the previous section we can estimate α and β directly from an image by counting the frequency of pixels with different values. For the derivation below we treat α and β as known although in practice we only have empirical estimates given by $\hat{\alpha}$ and $\hat{\beta}$. Now suppose w_0 , w_1 and ϵ_r are also known, and consider the problem of estimating θ_0 and θ_1 . Below we describe an algebraic method for estimating the appearance models.

Let $k = |L|$. We have $2k$ unknowns $\theta_0(1), \dots, \theta_0(k)$ and $\theta_1(1), \dots, \theta_1(k)$. Proposition 1 defines k linear and k^2 quadratic constraints,

$$\alpha(i) = w_0\theta_0(i) + w_1\theta_1(i). \quad (4)$$

$$\beta(i, j) = (w_0 - \epsilon_r)\theta_0(i)\theta_0(j) + (w_1 - \epsilon_r)\theta_1(i)\theta_1(j) + \epsilon_r\theta_0(i)\theta_1(j) + \epsilon_r\theta_1(i)\theta_0(j). \quad (5)$$

Minimal constraints We first consider a simple method that uses a subset of the constraints to solve for all of the unknowns in the appearance model. The approach uses the k linear constraints defined by α and k quadratic constraints defined by a single row of β .

1. Let $i \in L$. Using the quadratic constraint defined by $\beta(i, i)$ and the linear constraint defined by $\alpha(i)$ we can solve for $\theta_0(i)$ and $\theta_1(i)$,

$$\theta_0(i) = \alpha(i) \pm \frac{\sqrt{\beta(i, i) - \alpha^2(i)}}{\sqrt{\frac{w_0}{w_1} - \frac{\epsilon_r}{w_1^2}}}, \quad \theta_1(i) = \frac{\alpha(i) - w_0\theta_0(i)}{w_1}. \quad (6)$$

2. Now consider each $j \in L$ with $j \neq i$. Since we solved for $\theta_0(i)$ and $\theta_1(i)$ in Step 1, now $\beta(i, j)$ defines a linear constraint on $\theta_0(j)$ and $\theta_1(j)$. Together with the linear constraint defined by $\alpha(j)$ we can solve for both $\theta_0(j)$ and $\theta_1(j)$,

$$\theta_0(j) = \frac{w_1\beta(i, j) - \alpha(j)(w_1\theta_1(i) + \epsilon_r(\theta_0(i) - \theta_1(i)))}{(w_0w_1 - \epsilon_r)(\theta_0(i) - \theta_1(i))}, \quad \theta_1(j) = \frac{\alpha(j) - w_0\theta_0(j)}{w_1}. \quad (7)$$

3. We set $\theta_s(i) = \max(\theta_s(i), 0)$ and normalize θ_0 and θ_1 to add up to one.

Note that when $\beta(i, i) = \alpha^2(i)$ we have $\theta_0(i) = \theta_1(i)$. To avoid dividing by zero when solving for $\theta_0(j)$ in Step 2 and to increase the robustness of the method, we can select i maximizing $\beta(i, i) - \alpha^2(i)$ in Step 1. Note that if $\beta(i, i) - \alpha^2(i) = 0$ for all i then $\theta_0 = \theta_1 = \alpha$. Note also that to solve for $\theta_0(i)$ in Step 1 we require that $\beta(i, i) - \alpha^2(i) \geq 0$. Proposition 2 below shows that

$$\beta(i, i) - \alpha^2(i) = (w_0w_1 - \epsilon_r)(\theta_0(i) - \theta_1(i))^2. \quad (8)$$

Therefore $\beta(i, i) - \alpha^2(i) \geq 0$ when $w_0w_1 \geq \epsilon_r$. This leads to the requirement that for two pixels x and y with $\|x - y\| = r$, $P(x \in \mathcal{R}_s) \geq P(x \in \mathcal{R}_s | y \in \mathcal{R}_t)$, for $s \neq t$. For a fixed r , this constraint imposes certain conditions of the shape and size of \mathcal{R}_0 and \mathcal{R}_1 , restraining them from being too small and/or too narrow. As we shall see in Section 4.3 this constraint is satisfied in practice as long as r is not too large.

Least squares solution The approach described above only uses a small number of the constraints defined by β . In practice we have found that using all of the constraints in a least squares formulation leads to a more robust solution (recall that in practice we only have empirical estimates for α and β).

Let i_1, \dots, i_k be an ordering of $L = \{1, \dots, k\}$. Our empirical results show that ordering the indices in decreasing value of $\beta(i, i) - \alpha^2(i)$ works well and is better than a random order.

1. We start by solving for $\theta_0(i_1)$ and $\theta_1(i_1)$ using the approach defined above with the quadratic constraint defined by $\beta(i_1, i_1)$ and the linear constraint defined by $\alpha(i_1)$.
2. We iterate ℓ from 2 to k and solve for $\theta_0(i_\ell)$ and $\theta_1(i_\ell)$ in order of increasing ℓ . When solving for $\theta_0(i_\ell)$ and $\theta_1(i_\ell)$ we already have values for $\theta_0(i_1), \dots, \theta_0(i_{\ell-1})$ and $\theta_1(i_1), \dots, \theta_1(i_{\ell-1})$. Therefore $\beta(i_1, \ell), \dots, \beta(i_{\ell-1}, \ell)$ define $\ell - 1$ linear constraints on $\theta_0(i_\ell)$ and $\theta_1(i_\ell)$. Together with $\alpha(\ell)$ we form a system of ℓ linear equations with 2 unknowns that can be solved using linear least squares.
3. We improve our estimates by iterating ℓ from 1 to k and re-estimate $\theta_0(i_\ell)$ and $\theta_1(i_\ell)$ in each step. To re-estimate $\theta_0(i_\ell)$ and $\theta_1(i_\ell)$ we solve a linear least squares problem with k linear constraints and 2 unknowns. The linear constraints are defined by $\beta(i_\ell, j)$ for $j \neq i_\ell$ and $\alpha(i_\ell)$. Empirically we found that iterating over the entries one time using this method is enough to obtain improved results.
4. We set $\theta_s(i) = \max(\theta_s(i), 0)$ and normalize θ_0 and θ_1 to add up to one.

4.2 Spectral Method

Now we describe a spectral method for estimating the appearance models. As in the previous section we assume w_0 , w_1 and ϵ_r are known. The following proposition provides the basis for the approach.

Proposition 2.

$$\beta - \alpha\alpha^\top = (w_0w_1 - \epsilon_r)(\theta_0 - \theta_1)(\theta_0 - \theta_1)^\top \quad (9)$$

Proof. First note that $w_0 + w_1 = 1$ implies $w_0w_1 = w_0 - w_0^2$ and $w_0w_1 = w_1 - w_1^2$.

$$\begin{aligned} \beta - \alpha\alpha^\top &= (w_0 - \epsilon_r)\theta_0\theta_0^\top + (w_1 - \epsilon_r)\theta_1\theta_1^\top + \epsilon_r\theta_0\theta_1^\top + \epsilon_r\theta_1\theta_0^\top - (w_0\theta_0 + w_1\theta_1)(w_0\theta_0 + w_1\theta_1)^\top \\ &= (w_0 - \epsilon_r - w_0^2)\theta_0\theta_0^\top + (w_1 - \epsilon_r - w_1^2)\theta_1\theta_1^\top + (\epsilon_r - w_0w_1)\theta_0\theta_1^\top + (\epsilon_r - w_1w_0)\theta_1\theta_0^\top \\ &= (w_0w_1 - \epsilon_r)\theta_0\theta_0^\top + (w_0w_1 - \epsilon_r)\theta_1\theta_1^\top - (w_0w_1 - \epsilon_r)\theta_0\theta_1^\top - (w_1w_0 - \epsilon_r)\theta_1\theta_0^\top \\ &= (w_0w_1 - \epsilon_r)(\theta_0 - \theta_1)(\theta_0 - \theta_1)^\top \end{aligned}$$

□

The above result shows that that matrix $\beta - \alpha\alpha^\top$ is of rank one and its only eigenvector with non-zero eigenvalue is proportional to $(\theta_0 - \theta_1)$. The matrix $\hat{\beta} - \hat{\alpha}\hat{\alpha}^\top$ defines an approximation to $\beta - \alpha\alpha^\top$. Let v be the dominant eigenvector of $\hat{\beta} - \hat{\alpha}\hat{\alpha}^\top$ normalized so that $\|v\| = 1$. The vector v gives us an estimate of $(\theta_0 - \theta_1)/\|\theta_0 - \theta_1\|^2$. The corresponding eigenvalue λ can be used to estimate $(w_0w_1 - \epsilon_r)\|\theta_0 - \theta_1\|^2$. We can then estimate $\theta_0 - \theta_1$ as follows,

$$\theta_0 - \theta_1 = \sqrt{\frac{\lambda}{w_0w_1 - \epsilon_r}} v \quad (10)$$

The above equation along with Equation (2) and $\hat{\alpha}$ allow us to estimate θ_0 and θ_1 . Notice that we can use simple power iteration methods to compute this estimate. The algorithm complexity depends only on $|L|$, which is usually much lower than the number of pixels in the image.

We note that as in the algebraic method described in the previous section, the spectral method also requires that $w_0w_1 \geq \epsilon_r$. As discussed above and demonstrated in Section 4.3 this constraint is satisfied in practice as long as r is not too large.

4.3 Estimating w_0 , w_1 and ϵ_r

In order to approximate ϵ_r , we start from the assumption that the ground truth segmentation S is spatially coherent and that the boundary between regions ∂S is short, i.e., $|\partial S| \approx \sqrt{|\Omega|}$. In this case ϵ_r is proportional to the area within distance r from ∂S divided by $|\Omega|$, see Figure 2. In our experiments we set $r = \rho\sqrt{|\Omega|}$, where ρ is a parameter set by the user. This makes the selection of the distance r be adaptive to the image resolution. Our estimate of ϵ_r then becomes,

$$\epsilon_r = \kappa \frac{r\sqrt{|\Omega|}}{|\Omega|} = \kappa\rho. \quad (11)$$

Figure 3a shows the mean value of ϵ_r computed on the ground truth segmentations from the GrabCut dataset [1] for several values of ρ . From this data we estimate $\kappa = 0.47$ using linear regression. Figure 3b shows the fraction of images where $w_0w_1 \geq \epsilon_r$ on the ground truth segmentations in the GrabCut dataset. Note that when $\rho \leq 0.1$ the condition $w_0w_1 \geq \epsilon_r$, needed for both the algebraic and spectral estimation methods, is satisfied for *all* the images in the dataset. On the other hand, as ρ increases past 0.1, the condition is less frequently satisfied. This explains why the performance of the algorithms degrades for large values of ρ as shown in Section 5.

To estimate w_0 and w_1 we use the fact that $w_0 + w_1 = 1$ and simply search over possible values for w_0 . We consider a finite number of choices for w_0 in $(0, 1)$ and estimate appearance models for each choice. For each choice of w_0 and resulting appearance models (θ_0, θ_1) we compare β as defined by Equation (3) to the empirical $\hat{\beta}$ computed from the image. We select the model parameters minimizing $\|\beta - \hat{\beta}\|$.

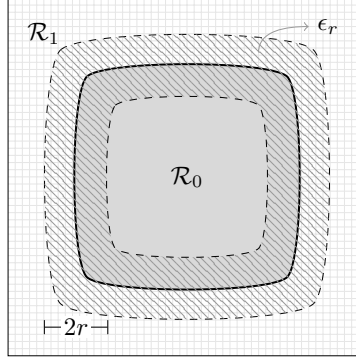


Figure 2: The area where pairs of pixels with $\|x - y\| = r$ can be in different regions.

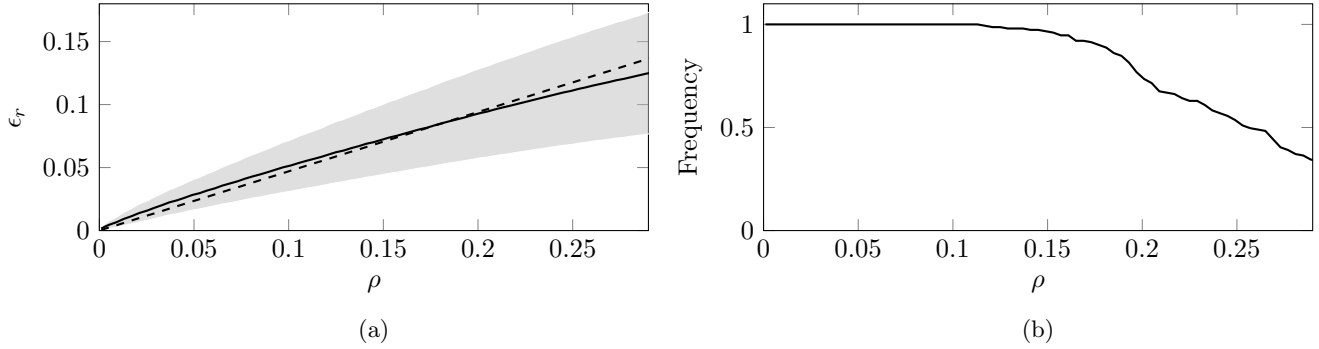


Figure 3: In (a) we show the mean (—) and standard deviation (▒) of ϵ_r as a function of ρ (see text). We also show the approximation for ϵ_r (---) defined by Equation (11). In (b) we show the fraction of images where $w_0 w_1 \geq \epsilon_r$ as a function of ρ . The images used here are from the Grabcut Dataset [1].

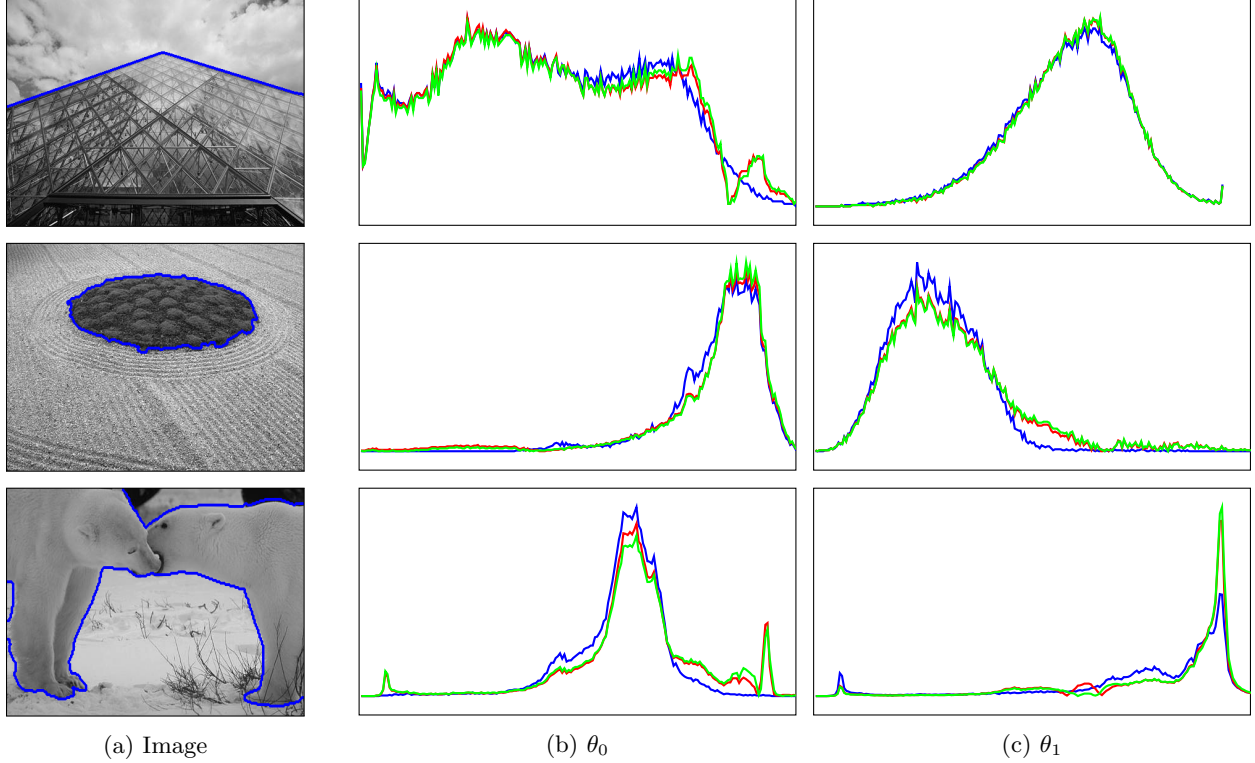


Figure 4: Estimation of appearance models with $\rho = 0.03$. In (a) we show the input images and their ground truth segmentation. In (b) and (c) we show the appearance models computed using the ground truth segmentation in blue (—), the algebraic method in green (—) and the spectral method in red (—). The images are from the Berkeley Segmentation [14] dataset.

4.4 Examples

Figure 4 illustrates some estimation results on real images for both the algebraic and spectral methods. For comparison we also show the appearance models computed using ground truth segmentations. For the case of a ground truth segmentation the appearance models are normalized histograms of the pixel values within each region. We see that both the algebraic and spectral methods give good results in these examples, leading to appearance models that are close to the ground truth.

5 Numerical Experiments

5.1 Evaluation Measures

To evaluate the quality of the appearance models we estimate we compare them to the appearance models defined by a ground truth segmentation using the Bhattacharyya distance,

$$d_B(p, q) = -\ln \left(\sum_{i \in L} \sqrt{p(i)q(i)} \right), \quad (12)$$

where p, q are discrete probability distributions over L .

Let I be an image with a ground truth segmentation defined by two regions \mathcal{R}_0 and \mathcal{R}_1 . Let θ_0 and θ_1 be the normalized histograms of the pixel values within each region. Let $\hat{\theta}_0$ and $\hat{\theta}_1$ be the appearance models estimated from I using one of our algorithms. We assess the quality of the estimates using a sum of two

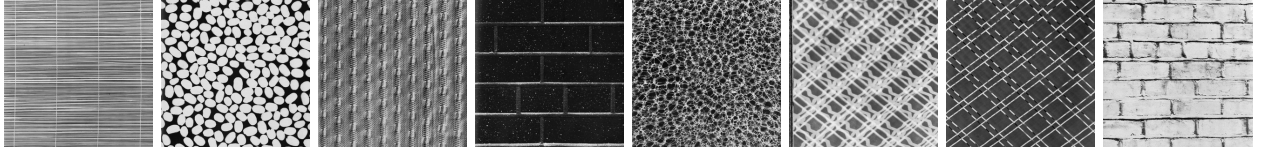


Figure 5: Selected Brodatz patterns

Bhattacharyya distances, allowing for a permutation of the region labels,

$$D_B = \min \left(\frac{d_B(\theta_0, \hat{\theta}_0) + d_B(\theta_1, \hat{\theta}_1)}{2}, \frac{d_B(\theta_0, \hat{\theta}_1) + d_B(\theta_1, \hat{\theta}_0)}{2} \right). \quad (13)$$

We will also evaluate the accuracy of segmentations obtained using the estimated appearance models by comparing them to the ground truth segmentations. We assess the overlap between two regions $J, Q \subseteq \Omega$ in different segmentations using the Jaccard index,

$$J(S, Q) = |S \cap Q| / |S \cup Q|.$$

Again let I be an image with a ground truth segmentation defined by \mathcal{R}_0 and \mathcal{R}_1 . Let \mathcal{Q}_0 and \mathcal{Q}_1 be the two regions obtained by segmenting I using the estimated appearance models. We compare the two segmentations using a sum of two Jaccard indices, again allowing for a permutation of the region labels,

$$\text{Jac} = \max \left(\frac{J(\mathcal{R}_0, \mathcal{Q}_0) + J(\mathcal{R}_1, \mathcal{Q}_1)}{2}, \frac{J(\mathcal{R}_0, \mathcal{Q}_1) + J(\mathcal{R}_1, \mathcal{Q}_0)}{2} \right). \quad (14)$$

All of our algorithms were implemented in Matlab and the experiments presented here were run on a Intel(R) Core(TM) i5-6200U CPU 2.30GHz with 8 Gb of RAM.

5.2 Synthetic Data

We first illustrate the result of series of experiments using synthetic data. To generate the synthetic data we used the ground truth segmentations in Figure 6 together with pairs of images defined as follows:

- IID: we used 50 pairs of random appearance models. For each appearance model we generate a 320×320 image where the pixel values are independent samples from the corresponding distribution.
- Brodatz: we selected all possible pairings from the Brodatz textures [13] depicted in Figure 5. We resized each image to be 320×320 pixels and applied a Gaussian filter with $\sigma = 1$ to remove artifacts.

For each pair of images defined above we use the four ground truth segmentation masks in Figure 6 to generate four images with two regions each. Figure 7 shows an example of the four images generated using two different Brodatz patterns.



Figure 6: Ground truth segmentations used to generate synthetic data.

5.3 Evaluating the effect of ρ

In Figure 8 we show the performance of our methods when estimating appearance models using various values of ρ with the synthetic data defined by the ground truth segmentations GT1 and GT2 (Figure 6).

Both of our algorithms almost perfectly recover the underlying appearance models for images where the pixels in each region are IID. In this case the methods work well over the whole range of values of ρ tested. This is expected since these images strictly follow both Assumption 1 and Assumption 2 and, therefore, provide the optimal setting for our algorithms.

For images with Brodatz textures Assumption 2 is violated for small values of ρ . As ρ increases the assumption is satisfied and the quality of our estimation improves. However, as ρ increases past a certain threshold, the quality of our estimators on images generated with GT2 decline, showing the potential problems that arise when ϵ_r is large (see Section 4.3).

5.4 Appearance Model Evaluation on Synthetic Images

We compare the performance of our methods to estimate appearance models to a variation of the alternation scheme described in [2], here called ALT.

In ALT, we start with an initial segmentation of the image and alternate between computing normalized histograms using the current segmentation and computing a new segmentation using the current appearance models. This procedure is iterated until convergence. To compute a new segmentation using the current appearance models we minimize the energy in Equation (1) using the usual max-flow based algorithms for graph cuts [9]. When computing appearance models we “smooth” the histograms of each region by adding a constant $K = 1$ to their bins before normalizing them.

For the experiments described here the initial segmentation used for ALT is defined by a square whose area is half of the total area of the image. Figure 9 shows an example of how the segmentation and appearance models evolve over time. Empirically, we found that ALT works well in some examples but a typical failure mode leads to assigning the whole image to single segment.

Table 1 compares the results of our methods to the result of ALT using several values of λ for the segmentation step. We used $\rho = 0.06$ (which corresponds to $r \approx 20$ pixels for the 320×320 synthetic images) for both the algebraic and spectral methods. Again notice that our algorithms perform extremely well on images where the pixel values are IID. The results on images with textures are also good and compare favorably to ALT. This result is compelling in particular because the proposed methods do not rely on an iterative model re-estimation scheme such as in ALT, which makes them faster and independent of initialization. The runtime of the different methods are shown in the last column of Table 1. Based on the results of these experiments we set $\lambda = 5$ for ALT in the experiments that follow.

5.5 Segmentation Evaluation on Synthetic Images

Having the estimated appearance models using either the algebraic or spectral methods we compute segmentations by minimizing Equation (1) using a max-flow algorithm for graph cuts [9]. We compared this approach to several existing texture segmentation methods.

Our methods were evaluated using $\rho = 0.06$ for estimating appearance models, and $\lambda = 5$ for the segmentation step.

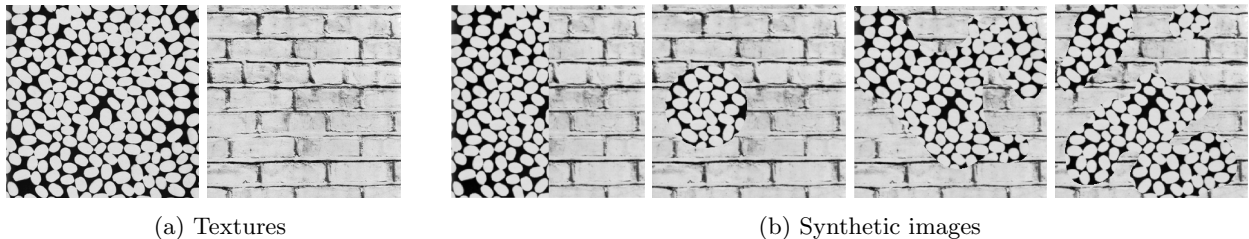


Figure 7: Examples of synthesized images with textures.

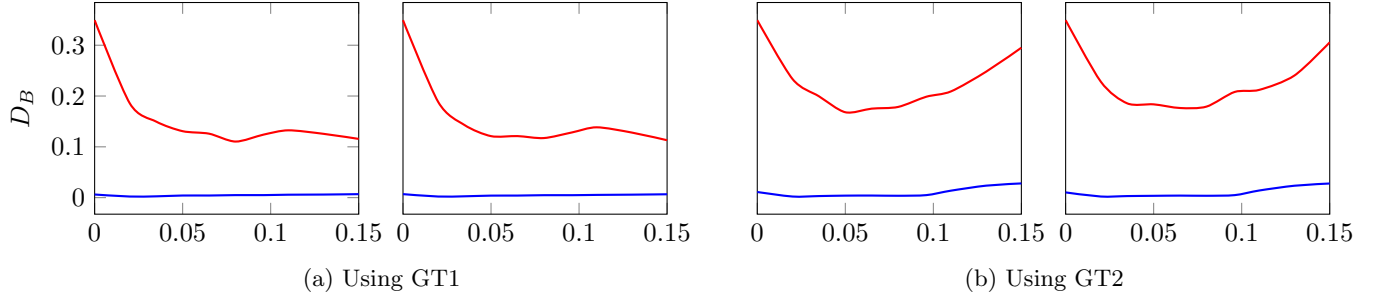


Figure 8: Average appearance model estimation error D_B as a function of ρ on images composed of IID (—) and Brodatz (—) patterns disposed as in GT1 and GT2. For both (a) and (b) the results on the left are due to the algebraic method, whereas the results on the right are from the spectral method.

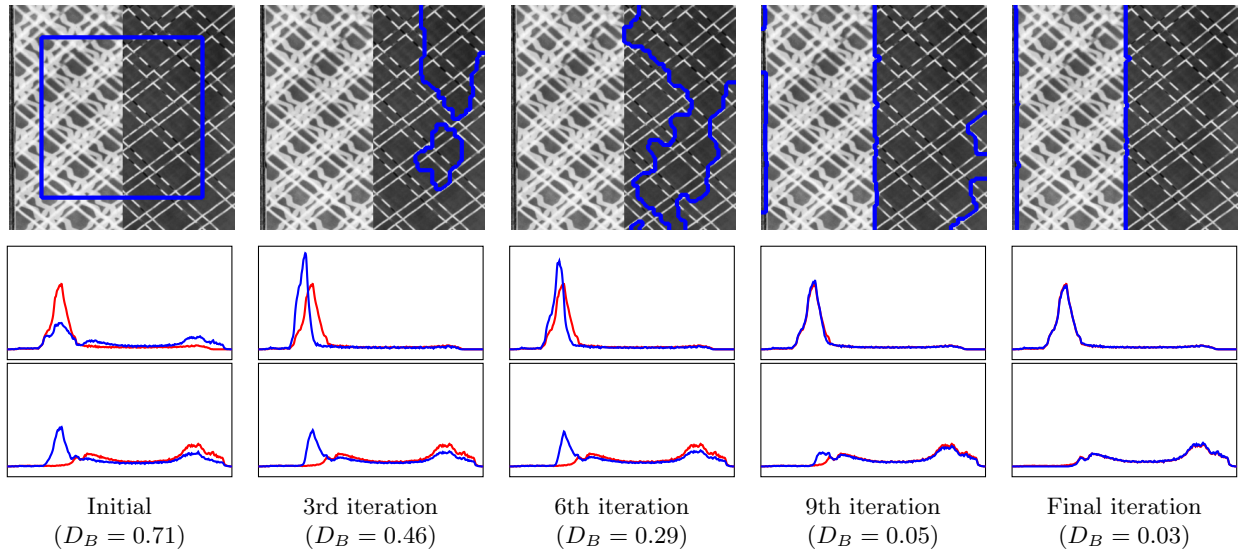


Figure 9: Model estimation and segmentation using ALT. On the bottom, we see how both foreground and background color distributions estimated by ALT (—) evolve compared to the ground truth appearance models (—). The evolution of the segmentations given the models is shown on top.

Table 1: Average D_B distance between estimated and ground truth appearance models on the synthetic data generated using different ground truth segmentations.

Method		Image Setting								Time (s)
		GT1		GT2		GT3		GT4		
		IID	Brodatz	IID	Brodatz	IID	Brodatz	IID	Brodatz	
Algebraic		0.001	0.036	0.002	0.106	0.003	0.039	0.003	0.066	0.94
Spectral		0.001	0.034	0.002	0.108	0.003	0.045	0.003	0.065	0.26
ALT	$\lambda = 1$	0.085	0.258	0.000	0.211	0.000	0.149	0.000	0.159	4.04
	$\lambda = 3$	0.083	0.035	0.000	0.038	0.000	0.029	0.000	0.073	4.38
	$\lambda = 5$	0.083	0.023	0.014	0.024	0.000	0.008	0.083	0.046	4.04
	$\lambda = 10$	0.083	0.096	0.061	0.044	0.046	0.017	0.083	0.091	3.87

Table 2: Jac index for the segmentation results using the same data as in Table 1.

Method	Image Setting								Time (s)
	GT1		GT2		GT3		GT4		
	IID	Brodatz	IID	Brodatz	IID	Brodatz	IID	Brodatz	
<i>Algebraic</i>	1.000	0.932	0.987	0.815	0.965	0.875	0.916	0.823	1.37
<i>Spectral</i>	1.000	0.934	0.987	0.813	0.965	0.865	0.912	0.820	0.70
ALT	0.503	0.873	0.943	0.875	0.949	0.903	0.512	0.820	3.22
LSWD	0.853	0.924	0.531	0.755	0.751	0.876	0.687	0.823	72.40
ORTSEG	0.825	0.933	0.694	0.831	0.750	0.882	0.774	0.836	1.66
FBS	0.567	0.901	0.516	0.767	0.567	0.832	0.544	0.816	0.10
PNMF	0.344	0.931	0.358	0.635	0.364	0.851	0.359	0.803	15.67

The existing methods we compare to include Level Set segmentation using Wasserstein Distances (LSWD) [4], Factorization Based Segmentation (FBS) [12], Projective Non-Negative Matrix Factorization on a Graph (PNMF) [15], and ORTSEG [11]. We also evaluate the results of ALT (described above).

The methods we have used for comparison have several similarities to our proposed algorithms. LSWD explicitly assumes local homogeneity. FBS, PNMf and ORTSEG make use of matrix factorization techniques to estimate appearance models in the form of histograms and make an implicit assumption of homogeneity. ALT deals directly with Equation (1). In addition to that, LSWD, FBS, PNMf and ORTSEG require the tuning of a window size parameter that has a function similar to r in our methods. For each of these methods, we used the provided Matlab implementations and tuned their parameters to improve their performance in our datasets.

Figure 10 illustrates some of the segmentations obtained using our approach and the above methods under both types of images used for evaluation, whereas Table 2 provides a quantitative evaluation on the full set of synthetic images generated using the procedure described in Section 5.2. This is the same data used to generate the results in Table 1. Notice that the runtime of our methods is increased for the segmentation experiments (Table 2) when compared to the model estimation experiments (Table 1) due to the addition of the graph cut computation on top of the appearance model estimation.

Table 2 demonstrates the superiority of our methods under the IID case. For the Brodatz setting, the results demonstrate that our methods can provide a satisfactory segmentation in many settings without relying on iterative approaches and Gabor filtering. This makes our methods faster than most of the other approaches, while still leading to highly accurate segmentations.

From these results we notice the importance of the assumptions presented in Section 3 and that high performance texture segmentation algorithms can be developed without the use of any kind of image filtering. As can be seen in the results in Figure 10 this leads to segmentations that are more accurate near region boundaries, where methods that rely on the response of filter banks often suffer. Finally, although not presented here for the sake of simplicity, our methods could have their segmentation performance further improved when using the estimated appearance as an initial guess for an iterative scheme such as ALT.

5.6 Real Images

We also tested the proposed algorithms on real images from a variety of datasets including the Berkeley Segmentation Dataset [14], the Plant Seedlings Dataset [16] and a Scanning Electron Microscope (SEM) dataset [17]. The images were chosen such that Assumption 1 approximately holds.

Figure 11 shows some of the segmentation results obtained using our two methods for estimating appearance models followed by segmentation using graph cuts. For each image, we used $\rho = 0.03$ and $\lambda = 5$. These results illustrate how the proposed algorithms work well on a variety of different types of images.

For these experiments, we added a preprocessing step to both methods in order to reduce the total number of colors in RGB images to a smaller number of quantized values. This step consisted on randomly partitioning the image color space until each partition has at most 1000 pixels. Starting from the whole set

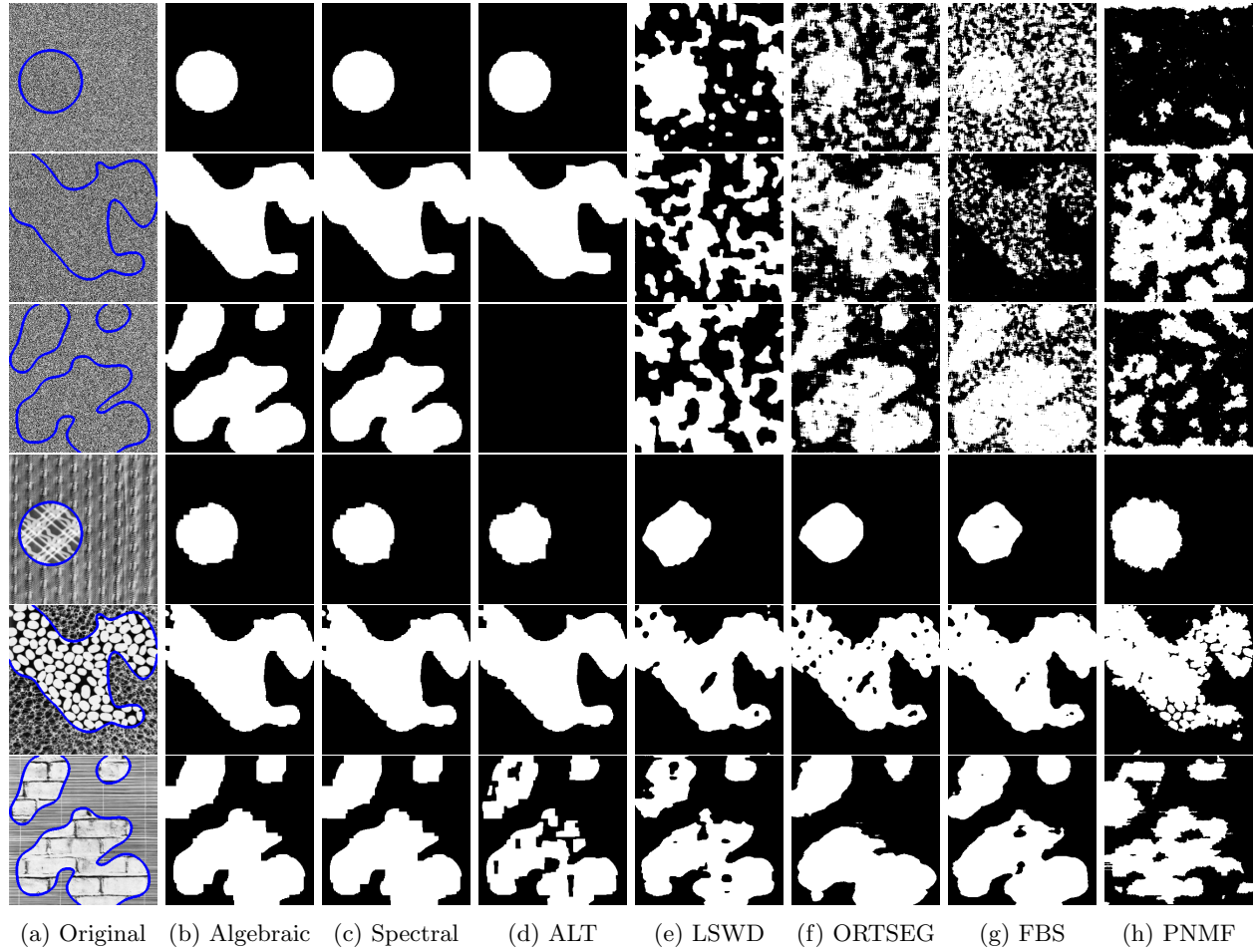
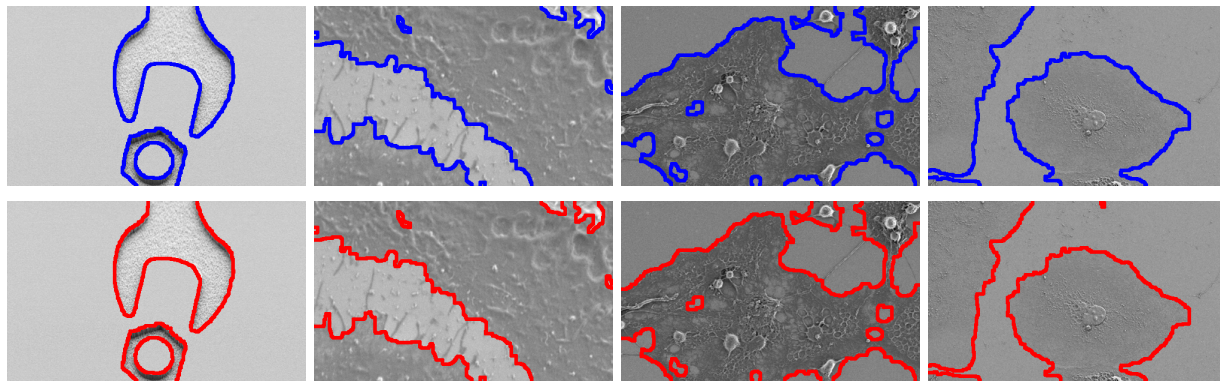
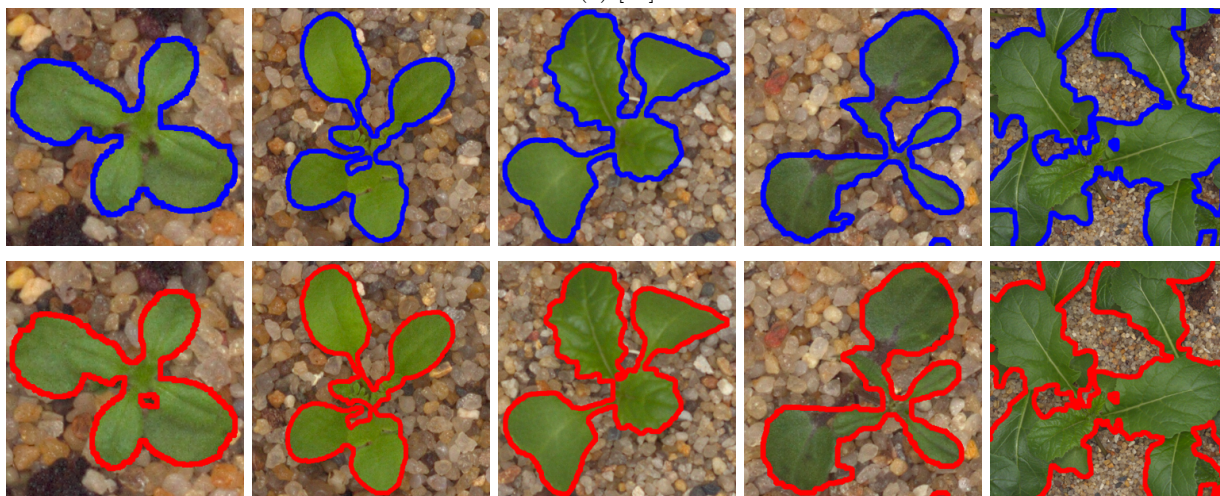


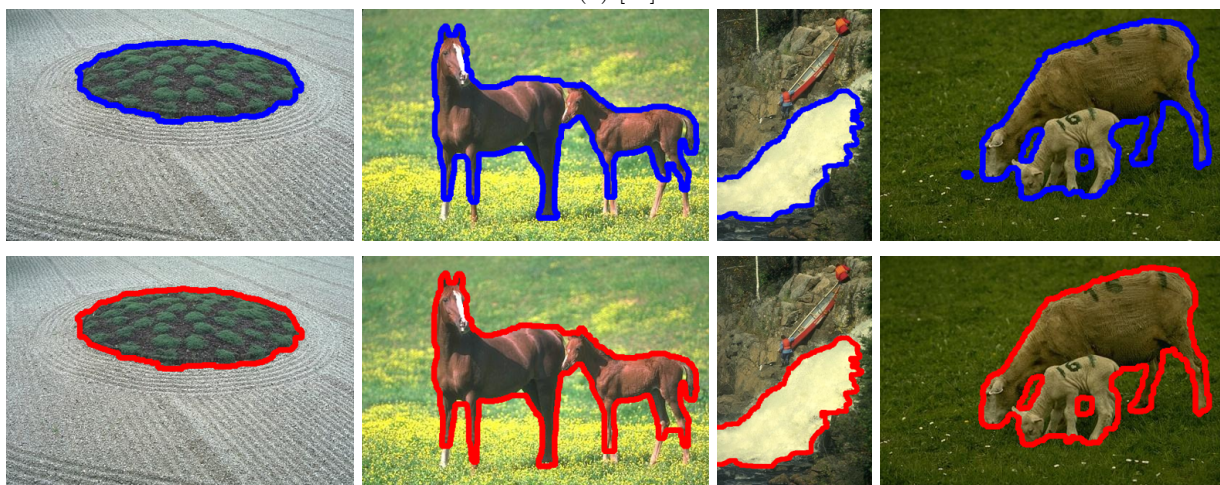
Figure 10: Selected segmentation results comparing our algorithms in (b) and (c) to other existing methods.



(a) [17]



(b) [16]



(c) [14]

Figure 11: Application our methods in natural scenes. The blue and red contours are the results of segmentation using appearance models estimated using the algebraic and spectral methods, respectively.

of pixels, we partition the set into two using a random hyperplane in RGB space going through the set's center of mass and then recur until the stopping criteria is met.

6 Conclusion

In this paper we addressed the problem of estimating appearance models for images with multiple regions. We showed that this can be accomplished without explicit reasoning about the set of pixels in each region. Instead, by assuming homogeneity of appearance within each region and independence at a distance we derived two methods for estimating the appearance of the unknown regions in an image. Our approach combines the distribution of pixel values within the whole image with the distribution of pairs of nearby values to obtain algebraic expressions that can be used to solve for appearance models. Our experiments demonstrate the proposed methods work well in a variety of settings and the resulting appearance models can be effectively used for segmentation of textured images. These results also suggest that segmentation algorithms can be improved by making use of second order pixel statistics.

References

- [1] Carsten Rother, Vladimir Kolmogorov, and Andrew Blake. Grabcut: Interactive foreground extraction using iterated graph cuts. In *ACM Transactions on Graphics*, volume 23, pages 309–314, 2004.
- [2] Meng Tang, Ismail Ben Ayed, and Yuri Boykov. Pseudo-bound optimization for binary energies. In *European Conference on Computer Vision*, pages 691–707, 2014.
- [3] Tony F Chan and Luminita A Vese. Active contours without edges. *IEEE Transactions on Image Processing*, 10(2):266–277, 2001.
- [4] Kangyu Ni, Xavier Bresson, Tony Chan, and Selim Esedoglu. Local histogram based segmentation using the wasserstein distance. *International Journal of Computer Vision*, 84(1):97–111, 2009.
- [5] Sara Vicente, Vladimir Kolmogorov, and Carsten Rother. Joint optimization of segmentation and appearance models. In *IEEE International Conference on Computer Vision*, pages 755–762, 2009.
- [6] Meng Tang, Lena Gorelick, Olga Veksler, and Yuri Boykov. Grabcut in one cut. In *IEEE International Conference on Computer Vision*, pages 1769–1776, 2013.
- [7] Julian Besag. On the statistical analysis of dirty pictures. *Journal of the Royal Statistical Society: Series B (Methodological)*, 48(3):259–279, 1986.
- [8] Dorothy M Greig, Bruce T Porteous, and Allan H Seheult. Exact maximum a posteriori estimation for binary images. *Journal of the Royal Statistical Society: Series B (Methodological)*, 51(2):271–279, 1989.
- [9] Yuri Boykov, Olga Veksler, and Ramin Zabih. Fast approximate energy minimization via graph cuts. In *IEEE International Conference on Computer Vision*, volume 1, pages 377–384, 1999.
- [10] Anil K Jain and Farshid Farrokhnia. Unsupervised texture segmentation using gabor filters. *Pattern recognition*, 24(12):1167–1186, 1991.
- [11] Michael T McCann, Dustin G Mixon, Matthew C Fickus, Carlos A Castro, John A Ozolek, and Jelena Kovacevic. Images as occlusions of textures: A framework for segmentation. *IEEE transactions on Image Processing*, 23(5):2033–2046, 2014.
- [12] Jiangye Yuan, Deliang Wang, and Anil M Cheriyyadat. Factorization-based texture segmentation. *IEEE Transactions on Image Processing*, 24(11):3488–3497, 2015.
- [13] Phil Brodatz. *Textures: a photographic album for artists and designers*. Dover Pubns, 1966.
- [14] D. Martin, C. Fowlkes, D. Tal, and J. Malik. A database of human segmented natural images and its application to evaluating segmentation algorithms and measuring ecological statistics. In *International Conference on Computer Vision*, volume 2, pages 416–423, July 2001.

- [15] Christos G Bampis, Petros Maragos, and Alan C Bovik. Projective non-negative matrix factorization for unsupervised graph clustering. In *IEEE International Conference on Image Processing*, pages 1255–1258, 2016.
- [16] Thomas Mosgaard Giselsson, Rasmus Nyholm Jørgensen, Peter Kryger Jensen, Mads Dyrmann, and Henrik Skov Midtiby. A public image database for benchmark of plant seedling classification algorithms. *arXiv preprint arXiv:1711.05458*, 2017.
- [17] Rossella Aversa, Mohammad Hadi Modarres, Stefano Cozzini, and Regina Ciancio. NFFA-EUROPE - SEM dataset, 2018.